J. Earth Syst. Sci. (2024)133 160
https://doi.org/10.1007/s12040-024-02366-4

Tectonomagmatic evolution of Khairagarh Group in Sitagota syncline, Dongargarh Supergroup, Bastar Craton: Insight into Paleoproterozoic crust mantle processes

Sunil Kumar Khare[1,*], Deepanker Asthana[2] and A S Venkatesh[2]

[1]*Department of Petroleum Engineering and Earth Sciences, University of Petroleum and Energy Studies, Dehradun 248 007, India.*
[2]*Department of Applied Geology, Indian Institute of Technology (Indian School of Mines), Dhanbad 826 004, India.*
[*]*Corresponding author. e-mail: sunilkhare2001@gmail.com*

MS received 22 May 2023; revised 16 March 2024; accepted 18 March 2024

This contribution presents for the first time a digital elevation map and 1:50,000 scale geological map of Sitagota syncline, Khairagarh Group, which is spread in around 1000 km^2 area in the north Bastar Craton (survey of India toposheets 64 C/11 and C/15). We report for the first time, exposures of Algoma-type banded iron formation, intertrappean shale, and oxide and sulphide mineralization in Mangikhuta basalt. Mafic enclaves are reported in the Dongargarh granite. Geochemistry and petrogenetic study of Mangikhuta and Kotima volcanics of Khairagarh Group is presented. Although field investigation and digital elevation map reveal Khairagarh volcano-sedimentary sequence underwent more than one phase of orogeny, the ubiquitous presence of very low-grade metamorphic mineral assemblages in volcanic rocks indicates they did not undergo high P–T transformation and most of the alteration and metamorphism took place at near-surface conditions. Our tectonomagmatic model proposes the occurrence of a rift basin in the north Bastar Craton from 2.46 to 2.2 Ga, resulting in sedimentation and high-Mg basalt to basaltic-andesite magmatism. The genesis of Sitagota syncline is attributed to closure and deformation of this rift basin due to compressive forces, probably related to Paleoproterozoic Dongargarh Kotri mobile belt and Mesoproterozoic central Indian tectonic zone. Tectonomagmatic and geochronological similarity of Khairagarh Group to Lower Wyloo Group of Ashburton basin in Pilbara Craton and Hekpoort and Ongeluk basalt formations of Transvaal basin in Kaapvaal Craton indicates Bastar Craton was part of Vaalbara supercontinent in Paleoproterozoic times.

Keywords. Bastar Craton; Dongargarh Supergroup; Paleoproterozoic; Khairagarh Group; basalt; rift basin; Vaalbara supercontinent.

1. Introduction

The Khairagarh Group is spread in approx. 1000 km^2 area towards W, NW, and SW of Khairagarh (21°25′15″N, 80°58′50″E) in Central India (Survey of India toposheets 64 C/11, C/12 and C/15). It is a constituent of the NNE–SSW trending Dongargarh Kotri mobile belt (DKMB) (Ramakrishna and Vaidyanathan 2010), and located south of the Central Indian Tectonic Zone (CITZ) (Yedekar

Published online: 17 August 2024

et al. 1990). The genesis of Paleoproterozoic (2.46–2.21 Ga) Khairagarh Group volcano-sedimentary succession has been attributed to rapid crustal growth of the north Bastar Craton (Sarkar 1957; Sarkar *et al.* 1994; Srivastava and Gautam 2009; Longjam and Talat 2012; Sensarma and Mukhopadhyay 2014; Manikyamba *et al.* 2016; Khanna *et al.* 2019) near Archean Proterozoic transition. Tectonomagmatic study of Khairagarh Group assumes special importance due to its temporal proximity to global Neoarchean Paleoproterozoic phenomena of onset of mature plate tectonics (c.f. Condie and Kroner 2008; Cawood *et al.* 2018; Hawkesworth and Brown 2018; Windley *et al.* 2021). Since Khairagarh volcanic formations exhibit alteration and very low-grade regional metamorphism (Asthana *et al.* 1996; Patel *et al.* 2008; Khanna *et al.* 2019; Khare and Asthana 2020; Khare *et al.* 2022), they provide a unique opportunity to undertake reliable geochemical and petrogenetic study to elucidate crust mantle processes responsible for Paleoproterozoic crustal evolution of north Bastar Craton. There is temporal and spatial proximity of Khairagarh volcanism to Malanjkhand (22°00′54″N; 80°42′36″E) Cu ± Mo ± Au metallogeny (Sikka and Nehru 1997; Kumar and Rino 2006; Pandit and Panigrahi 2012; Nehru and Sikka 2014; Pandit *et al.* 2014; Kumar and Asthana 2018; Arya *et al.* 2021). Therefore, it becomes imperative to undertake field geological, geochemical and petrogenetic study of Khairagarh volcanic formations and look for any evidence which indicates a relationship between Khairagarh volcanism and Malanjkhand metallogeny.

With this context, in this contribution, we present for the first time a detailed 1:50,000-scale geological map of Khairagarh Group, which is well exposed in Sitagota syncline. Our work presents a digital elevation map (DEM) of syncline prepared on ArcGIS software. We report the presence of faults in the syncline not reported earlier. Algoma-type BIF and intertrappean shale beds are reported in the Mangikhuta basalt of the Khairagarh Group. Magmatic oxide and sulphide mineralization is also reported in the Mangikhuta basalt. We report the presence of mafic enclaves in Dongargarh granite, which is the basement of the Khairagarh Group. Geochemical and petrogenetic study is presented for the Mangikhuta and Kotima volcanic formations, and a tectonomagmatic model presented for the genesis of the Khairagarh Group. A post-deposition orogenic model of Khairagarh Group is presented in this work.

2. Regional geology

Bastar Craton is an important Archean province of peninsular India, which lies to the south of Central Indian Tectonic Zone (CITZ) (Yedekar *et al.* 1990), and surrounded from the east and west by Singhbhum and Dharwar cratons, respectively (figure 1a) (Radhakrishna and Naqvi 1986; Naqvi and Rogers 1987; Mondal *et al.* 2006). The Dongargarh Supergroup, an important constituent of Bastar Craton is a Neoarchean–Paleoproterozoic succession of granite intrusions, bimodal volcanic formations, and volcano-sedimentary sequence spanning a 90 km wide and 150 km long NNE–SSW trending belt between Sakoli and Chhattisgarh basin in Central India (figure 1b) (Sarkar 1957, 1994; Mohanty 2015). The constituents of Dongargarh Supergroup are Nandgaon bimodal basalt and rhyolite formations, Dongargarh granite and Khairagarh Group (Rao 1981; Krishnamurthy *et al.* 1990; Neogi *et al.* 1996; Khanna *et al.* 2019; Santosh *et al.* 2020). Detailed chronostratigraphic succession of the Dongargarh Supergroup is given in table 1. The Khairagarh Group is around 12-km thick volcano-sedimentary sequence, which unconformably overlies above Dongargarh granite and Nandgaon bimodal volcanics. Sarkar (1957, 1958) published the geological map of Dongargarh System (figure 1c), which included map of Khairagarh Group from faulted western limb of Sitagota syncline (toposheet 64 C/12). However, a major portion of syncline towards north–northeast (toposheet 64 C/11 and C/15) remained unmapped due to inaccessible terrain. Rao (1981) published a regional map of Malanjkhand extension area which included the Sitagota syncline but detail mapping of Khairagarh volcanics and sediments towards centre of the Sitagota syncline (toposheet 64 C/11 and C/15) was not done. Later, several workers studied Dongargarh Supergroup (Sarkar *et al.* 1981; Krishnamurthy *et al.* 1990; Sarkar *et al.* 1994; Asthana *et al.* 1996, 1997, 2001; Neogi *et al.* 1996; Ghosh *et al.* 2006; Longjam and Talat 2012; Sensarma and Mukhopadhyay 2014; Khanna *et al.* 2019; Santosh *et al.* 2020). However, none of these studies reported detailed geology and field relations of volcanics and sediments from the centre of Sitagota syncline, which is part of our current work.

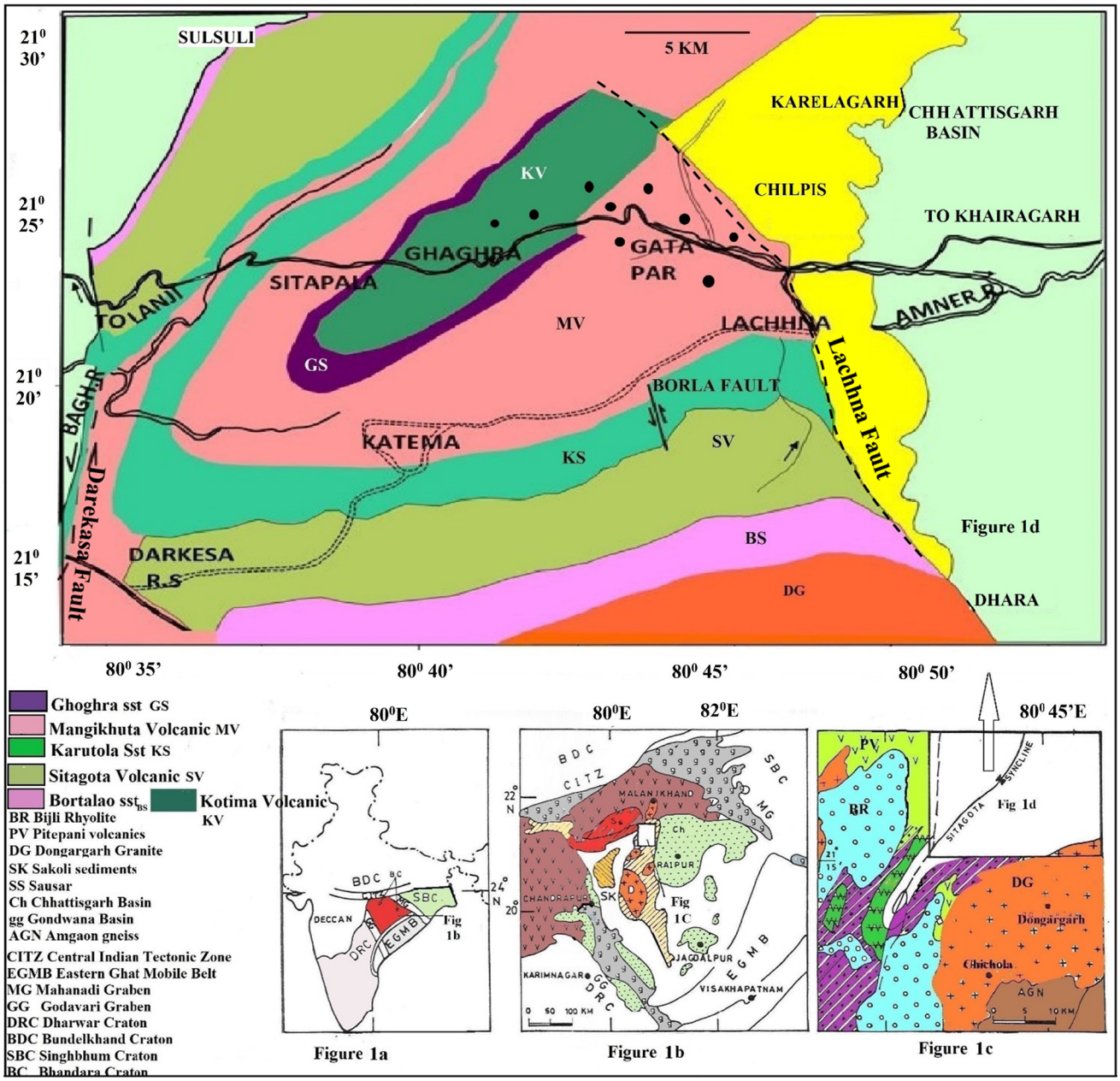

Figure 1. A geological map prepared after detailed field investigation of Sitagota syncline. **(a)** shows the location of Bastar Craton (BC) in Peninsular India vis-a-vis CITZ and other Archean cratons (Radhakrishna and Naqvi 1986). **(b)** shows the overall geology of Bastar Craton and location of the Dongargarh Supergroup in Bastar Craton (Kumar and Asthana 2018). **(c)** is geological map of Dongargarh Supergroup after Sarkar (1957). This map shows unmapped NE portion of Sitagota syncline. **(d)** is a geological map of Sitagota syncline made during the course of current field study. Black circles show location of samples collected for geochemical studies.

3. Field geology of Sitagota syncline

The Nandgaon bimodal volcanics and Dongargarh granite form the basement of Khairagarh Group. The outcrops of Dongargarh granite (figure 2a) are well exposed in and around Dongargarh (21°10′37″N; 80°45′04″E). The Pitepani basalt (figure 2b) and Bijli rhyolite (figure 2c) of Nandgaon Group are well exposed in Pitepani (21°09′55″N; 80°35′12″E) and Bagrekasa (21°08′54″N; 80°34′26″E), respectively. Dark grey-coloured, micro-granular mafic enclaves are present in Dongargarh granite outcrops (figure 2d), which could be either remnants of underlying Pitepani basalt or a product of magma mixing and assimilation. One km north of Dhara (21°15′45″N; 80°51′03″E), a 50-m thick conglomerate horizon in lower portion of Bortalao Formation establishes an

Table 1. *Chronostratigraphic succession of Dongargarh Supergroup and Khairagarh Group in Sitagota syncline after Rao (1981) and Sarkar (1994). The geochronology data taken from Krishnamurthy et al. (1990), Manikyamba et al. (2016) and Khanna et al. (2019). The thickness of volcanic and sedimentary units in Sitagota syncline estimated during the course of the current study.*

Dongargarh Supergroup

Chandarpur Sandstone
----------***Unconformity*** ----------
Kotima Volcanic (~1500 m)
----------*Unconformity?* ----------
Ghoghra Sandstone (~500 m) (~2210 Ma)
----------*Unconformity?* ----------
Mangikhuta Volcanic (~3000 m)
Khairagarh Group (~2.2 Ga U-Pb) -------*Unconformity* ----------
Karutola Sandstone (~1000 m) (~2453 Ma)
----------*Unconformity* ----------
Sitagota Volcanic (~5000 mt)
----------*Unconformity* ----------
Bortalao Formation (~1000 mt) (~ 2463 Ma)
---------- ***Unconformity*** ----------
Dongargarh Granite (~ 2.5 Ga U-Pb Zircon)
Pitepani Volcanic
Nandgaon Group (~2.5 Ga) ----------*Unconformity?* ----------
Bijli Rhyolite (~ 2.5 Ga U-Pb)
----------***Unconformity (Amgaon Orogeny)*** ----------
Amgaon gneiss (~3.4 Ga)

unconformable relationship between Dongargarh granite and Khairagarh Group (figure 2e). Conglomerate outcrops of Bortalao Formation are also seen near Bortalao (21°13′33″N; 80°36′57″E) along Dongargarh Darekasa Road (figure 2f). Khairagarh volcano-sedimentary sequence consists of Sitagota, Mangikhuta and Kotima basalt formations, respectively, overlying Bortalao, Karutola and Ghoghra sandstone formations (figure 1d). Bortalao Formation occurs as a prominent sandstone ridge near Dhara (figure 2g). The Sitagota basalt outcrops (figure 2h) are seen between Bortalao and Darekasa near Jamakudo (21°15′26″N; 80°35′36″E). During a traverse along Khairagarh Lanji Road, the outcrops of Mangikhuta basalt are exposed in the nallah section near Temri (21°23′39″N; 80°47′23″E). The Khairagarh volcanic formations occur as dispersed outcrops between sandstone ridges. They are fresh green to greenish grey coloured, non-schistose and devoid of pillow structures. Intertrappean shale of 5–10 m thickness is present in Mangikhuta basalt. Although flow layers are not evident in the field, quartz and calcite-filled vesicles and amygdules easily identify them (figure 2i). A 10-m thick Algoma-type banded iron formation (BIF) was discovered in intertrappean shales in Mangikhuta basalt near the contact of Karutola and Mangikhuta formations. The BIF extends for nearly 30–40 m and consists of alternate meso to micro clay and iron-rich bands. The maturity of Khairagarh sediments progressively increases from lower Bortalao to upper Ghoghra Formation. Field study indicates that the Ghoghra Formation pinches out laterally in both limbs of the syncline, and underlying Mangikhuta basalt continues without any overlying sediments into the Kotima basalt in the centre of the syncline (figure 1d). Khairagarh volcano-sedimentary sequence was gently folded (dips varying from 10° to 45°) to give rise to a regional NNE–SSW trending syncline structure spread in survey of India toposheets 64 C/11 and 64 C/15. The western limb of the Sitagota syncline was sinistrally displaced southwards (toposheet 64 C/12) by the 'Great Darekasa Fault' (figure 1d, Sarkar 1957).

Towards the east, the syncline abuts against buff-coloured, NS trending and vertical dipping beds of the Chilpi Group (figure 2j, Rao 1981). This contact between Khairagarh Group and the Chilpi Group is a major fault, which is evident from occasional brecciated and silicified outcrops from Dhara to Karelagarh (figure 1d). Due to its prominent exposure near Lachhna, we name this fault as 'Lachhna Fault'. A NS trending sinistral 'Borla Fault' was traced in the field, which runs parallel to Lachhna Fault (figure 1d).

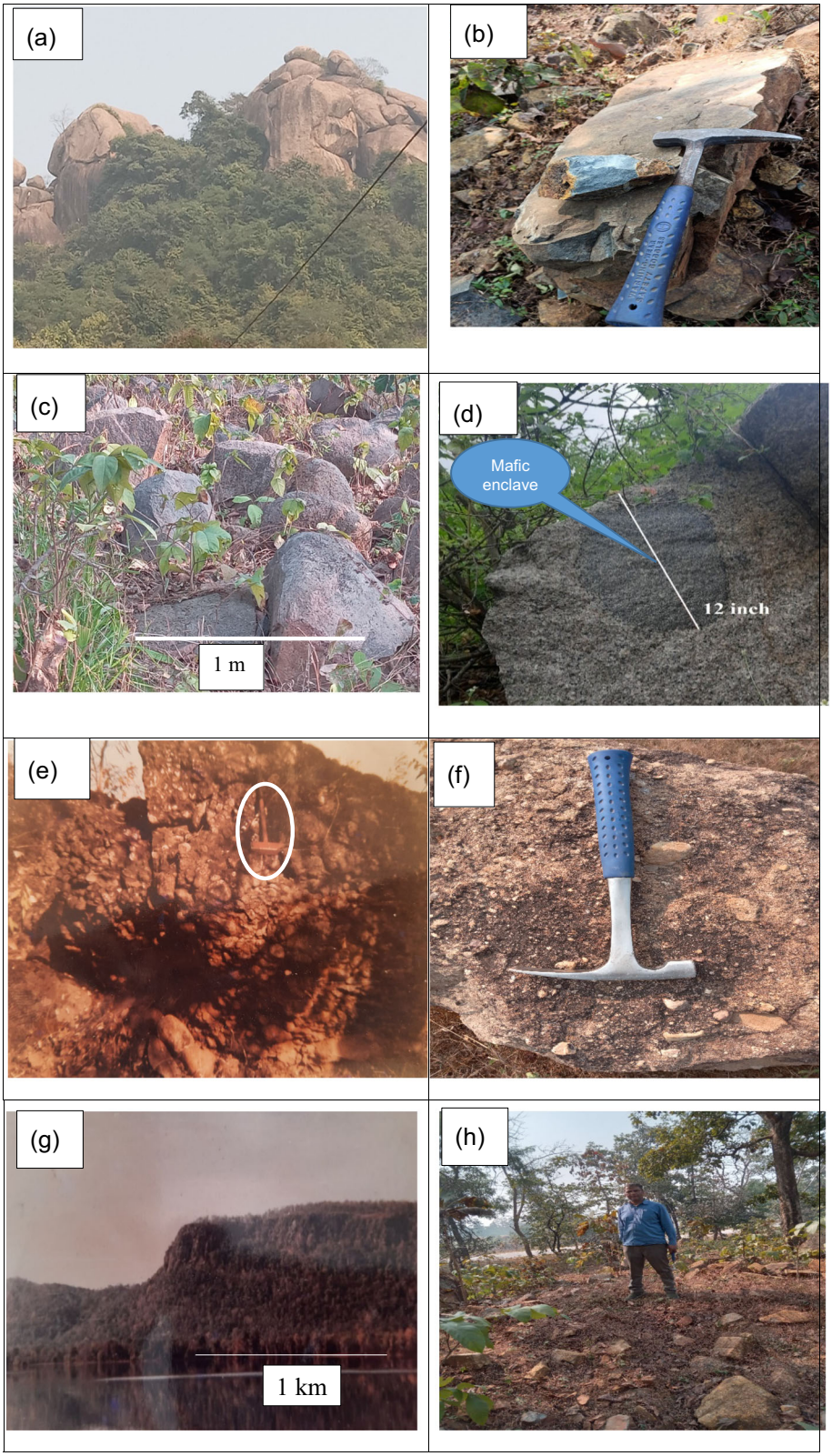

Figure 2. Pictures of geological features in and around Sitagota syncline. **(a)** Dongargarh granite batholith outcrops in Dongargarh. **(b)** A visual of fresh Pitepani basalt sample taken from Pitepani village. **(c)** Bijli rhyolite outcrops near Bagrekasa village. **(d)** Mafic enclaves seen in Dongargarh granite outcrop located in Dongargarh town. **(e)** Bortalao Basal conglomerates present near Dhara. **(f)** Conglomerate horizon near Bortalao railway station along Dongargarh Darekasa road. **(g)** Bortalao sandstone ridge seen from Dhara water tank. **(h)** Sitagota basalt outcrops near Dongargarh Darekasa road. **(i)** Vesicles seen in Mangikhuta basalt. **(j)** Chilpi shale outcrops along Khairagarh Lanji road near Lachhna.

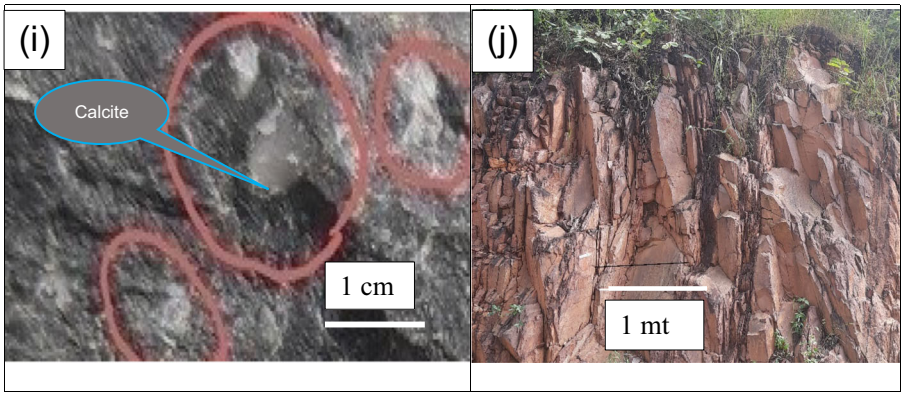

Figure 2. (*Continued.*)

4. Digital elevation map

Figure 3 is a digital elevation map (DEM) of Sitagota syncline, and its adjacent area prepared from United States Geological Survey (USGS) earth explorer digital data of terrain. The digital data was plotted on ArcGIS Arc Scene application to get a DEM of Sitagota syncline. DEM represents absolute vertical elevation of the earth surface that excludes any surface objects and has vertical accuracy of around 0.82 m (www.usgs.gov). DEM reveals volcano-sedimentary sequence underwent more than one phase of compression and orogeny post its deposition. Syncline is elevated towards the centre with a maximum elevation of around 800 m (2625 ft). The red-labelled elevations (>600 m) show a regional NS trend irrespective of formations of the Khairagarh Group, which indicates an EW compressive force probably acted on the volcano-sedimentary sequence giving rise to a NS trending dome/anticline structure.

5. Geochemistry of Khairagarh volcanics

5.1 *Petrography*

Petrography of Mangikhuta and Kotima volcanic samples collected from the centre of the syncline reveals the presence of quenched, sub-variolitic, and subophitic-to-ophitic relict igneous textures. Vesicles are filled with chalcedony and calcite (figure 4a). Some samples show pseudomorphs after olivine (?) in a matrix of quenched pyroxenes and plagioclase, indicating relict porphyritic textures (figure 4b). Flow top samples reveal relict quenched texture (figure 4c). Interior of the flow samples reveal subophitic to ophitic relict igneous textures where prismatic altered euhedral crystals of plagioclase are partially to completely enclosed by fresh magmatic clinopyroxenes, which indicates cotectic precipitation of clinopyroxene and plagioclase (figure 4d). Plagioclase occurs both as microphenocrysts and in groundmass, shows twinning and occasional sericitization. The glassy matrix is altered to secondary mineral aggregate consisting of chlorite, zoisite, clinozoisite, prehnite and pumpellyite. Few samples contain a good number of opaque minerals that occur randomly throughout the section. The reflected light study of opaque minerals indicates they are typical magmatic oxides predominantly Ti-magnetite, skeletal magnetite, vanadiferous magnetite, ilmenite, and hematite (figure 4e). Other than these typical magmatic oxide mineral assemblages, some sulfide minerals like pyrrhotite, pyrite and chalcopyrite grains are also seen in some samples (figure 4f) (c.f. Khare *et al.* 2024).

5.2 *Whole rock analytical techniques*

Nine non-vesicular, unweathered, fine-grained and least altered Mangikhuta and Kotima volcanic samples collected from Sitagota syncline (location given in figure 1d) were chosen for whole-rock geochemical analyses. Major oxides and trace element concentrations were measured on a Wavelength Dispersive X-ray Fluorescence Spectrometer (WD-XRF; Bruker, Tiger S8) at the Wadia Institute of Himalayan Geology (WIHG), Dehradun, India. Precision of analysis is estimated to be ±2–3% for major oxides and ±5–6% for trace elements. Rare earth elements (REE) and selected trace element concentrations were analyzed with Perkin-Elmer SCIEX ELAN DRC-e Inductively Coupled Plasma Mass Spectrometer (ICP-MS) at WIHG, Dehradun. Accuracy from 2 to 12%, and precision varying from

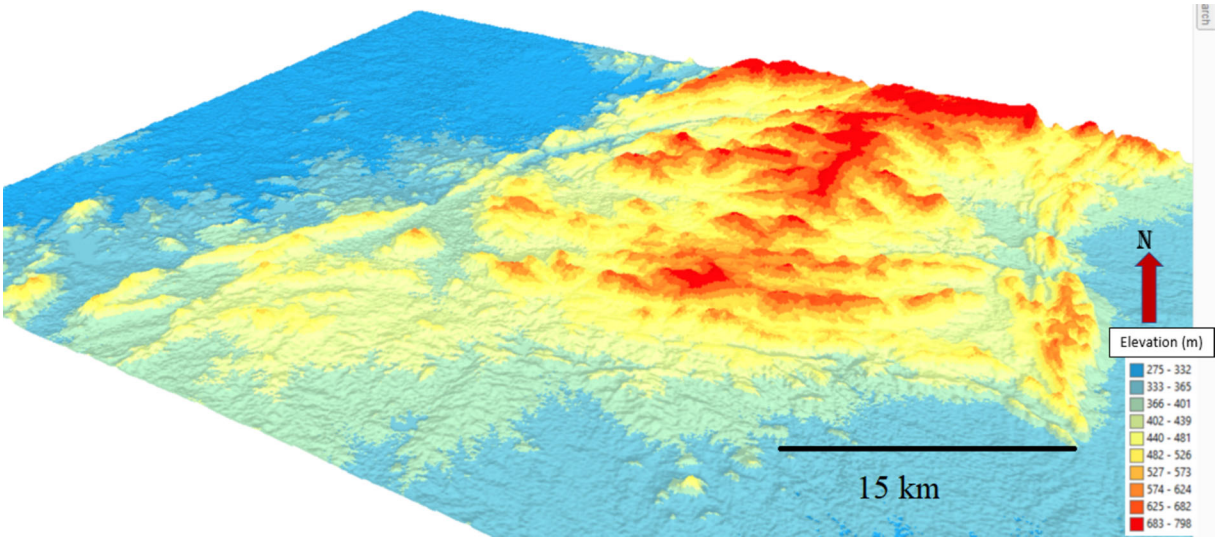

Figure 3. Digital elevation map of Sitagota syncline plotted on ArcGIS from terrain digital data downloaded from USGS earth explorer.

1 to 8% were obtained. Details of whole rock XRF and ICP-MS analytical techniques are given elsewhere (c.f. Saini *et al.* 2000; Khanna *et al.* 2009). Whole rock major, trace, LOI, REE composition and CIPW norm of the Khairagarh volcanic samples are given in table 2.

5.3 *Geochemistry*

CIPW norm mineralogy reveals all Khairagarh volcanic samples chosen for analysis are quartz normative. Plagioclase, orthopyroxene, clinopyroxene, orthoclase, and Fe-oxide are the other major precipitating minerals inferred from norm mineralogy. Total alkali content of Khairagarh volcanics is low ($Na_2O + K_2O < 4.17$ wt%), indicating their sub-alkaline nature. SiO_2 content from 51.19 to 55.25 wt% indicates basalt to basaltic andesite composition. On the TAS plot of Cox *et al.* (1979), Khairagarh volcanics plot in the field of sub-alkali basalt, basaltic andesite to andesite (figure 5). Low Nb (<10 ppm) and low Nb/Y ratios (0.1–0.4) corroborate their sub alkaline tholeiitic to calc-alkaline nature (Pearce and Cann 1973; Winchester and Floyd 1977; Hastie *et al.* 2007). On Nb/Y *vs.* Zr/Ti plot after Pearce (1996), Khairagarh volcanics plot in the field of sub-alkali basalt to basaltic andesite (figure 6). TiO_2 content is overall low (0.48–0.76 wt%), which indicates they belong to the low-Ti suite of Asthana *et al.* (1996). MgO content is high (6.9–11.2 wt%) while Al_2O_3 is relatively low (9.15–14.01 wt%). On Al_2O_3 *vs.* MgO plot after Kersting and Arculus (1994), Khairagarh volcanics plot in the field of high-Mg basalt (figure 7), similar to Boninite like composition reported from modern day arcs (Murton 1989; Taylor *et al.* 1994; Li *et al.* 2022). CaO varies from 4.8 to 10.9 wt%, while FeO(T) varies from 10.2 to 11.6 wt%. On the AFM plot after Winchester and Floyd (1977), Khairagarh basalt shows a moderate iron enrichment trend indicating tholeiitic to transitional affinity (figure 8). However, on TYC plot after Davies *et al.* (1979), they show characteristic transitional to calc-alkaline trend (figure 9). Due to immobility of Cobalt and Th in altered rocks, Co *vs.* Th plot (Hastie *et al.* 2007) is drawn for Khairagarh basalt (figure 10). On this plot, which acts as proxy to K_2O–SiO_2 plot, Khairagarh volcanics plot in calc-alkaline field. Therefore, based on relatively immobile element plot findings, we assign transitional to calc-alkaline affinity to Khairagarh volcanics. Overall, the whole rock composition indicates sub-alkaline, low-Ti, high Mg tholeiitic, transitional to calc-alkaline basalt-basaltic-andesite to andesite composition of Khairagarh volcanics.

The chondrite-normalized REE plot is drawn for Khairagarh volcanics (figure 11) with normalization values taken from McDonough and Sun (1995). The plot shows moderate LREE enrichment with respect to HREE. $(La/Sm)_N$ varies from 2 to 3.4, which indicates moderate enrichment of LREE with respect to MREE either due to magma source enrichment with an LREE-enriched melt/fluid or enrichment of LREE due to magma fractionation. $(Gd/Lu)_N$ varies from 1.3 to 1.8 indicating least

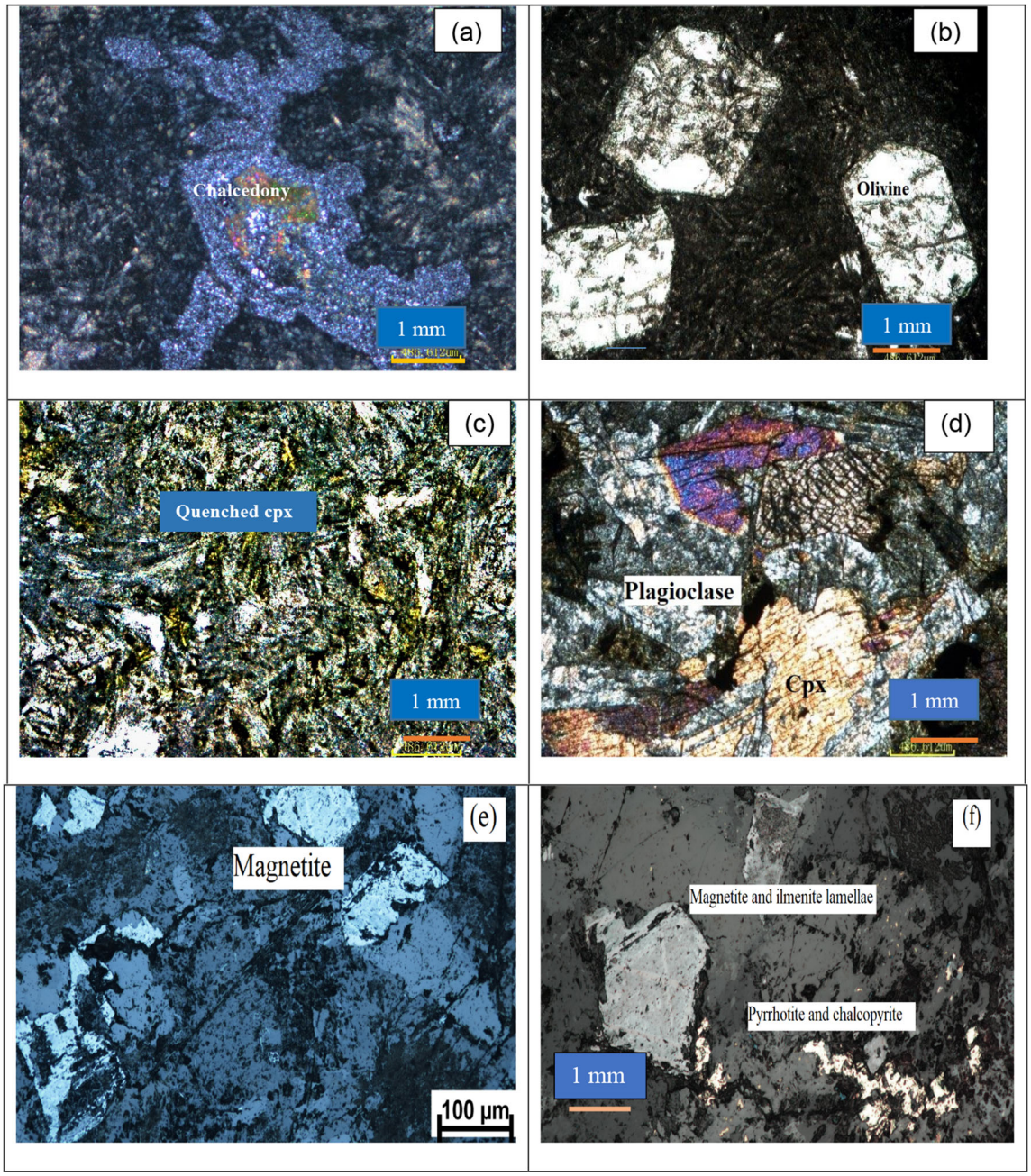

Figure 4. Photomicrographs of Khairagarh volcanics in transmitted **(a, b, c, d)** and reflected **(e, f)** light. **(a)** Photomicrograph (×10) of Khairagarh volcanics showing presence of chalcedony as vesicle filling mineral. **(b)** Pseudomorphs after olivine (?) in a quenched groundmass forming relict porphyritic texture. **(c)** Photomicrograph (×10) of quenched textures obtained from Khairagarh volcanics flow top, formed due to rapid cooling of lava on surface that led to formation of dendritic pyroxene grains. **(d)** Grains of fresh unaltered pyroxenes, altered plagioclase and opaques showing sub-ophitic to ophitic relict textures (×10). **(e)** A reflected light photomicrograph showing typical euhedral magnetite grains exhibiting skeletal to exsolution features with laths of ilmenite occupying the octahedral cleavage planes of magnetite. **(f)** A reflected light photomicrograph showing magnetite grain along with ilmenite lamellae as an exsolution feature substituting the octahedral cleavage of magnetite. Other minerals include aligned pyrrhotite and chalcopyrite as ductile assemblages.

impact of fractionation and partial melting on their relative abundance. Negative Eu anomaly indicates plagioclase fractionation from the melt, also evident from petrography and normative mineralogy.

6. Nature of mantle source

HFSE ratios remain unchanged due to various degrees of partial melting, fractional crystallization, alteration, and low-grade metamorphism;

Table 2. *Whole rock major, trace and REE analysis data of Khairagarh volcanic samples collected from centre of syncline, location given in figure 2(d). Normative mineralogy is given in the table.*

Sample #	SK13	SK14	SK16	SK17	SK18	SK20	SK21	SK31	SK37
SiO_2	55.02	54.36	54.65	54.78	52.87	51.19	51.78	52.93	55.25
TiO_2	0.65	0.68	0.68	0.67	0.64	0.72	0.48	0.76	0.75
Al_2O_3	13.55	13.63	14.01	13.38	14.10	12.83	9.15	13.50	12.89
Fe_2O_3	10.33	11.12	11.07	10.74	10.83	11.49	11.61	11.45	10.18
MnO	0.15	0.17	0.17	0.15	0.17	0.19	0.18	0.18	0.16
MgO	6.93	7.46	7.39	7.22	7.72	11.06	11.23	11.00	9.96
CaO	7.84	7.63	8.06	7.69	9.05	6.69	12.91	4.80	5.75
Na_2O	1.36	1.90	2.11	1.62	2.11	2.12	1.11	2.01	2.24
K_2O	2.16	0.97	0.73	1.30	0.86	1.21	1.03	1.00	1.13
P_2O_5	0.09	0.08	0.09	0.08	0.07	0.09	0.05	0.08	0.08
Total	**98.08**	**98.00**	**98.96**	**97.63**	**98.42**	**97.59**	**99.53**	**97.71**	**98.39**
L.O.I.	2.53	2.75	2.60	2.72	2.71	4.09	4.06	4.11	3.26
Normative mineralogy									
Quartz	14.93	14.82	14.29	16.00	10.47	5.96	9.35	10.94	12.29
Plagioclase	36.00	41.87	44.45	39.10	44.32	39.86	26.33	40.30	40.73
Orthoclase	12.76	5.73	4.31	7.68	5.08	7.15	6.09	5.91	6.68
Diopside	9.44	7.64	8.62	8.44	12.61	6.77	27.77	0.00	3.13
Hypersthene	12.81	15.04	14.41	14.07	13.38	24.41	15.10	27.40	23.36
Olivine	0.00	0.00	0.00	0.00	0	0.00	0.00	0.00	0.00
Ilmenite	0.31	0.35	0.35	0.52	0.24	0.29	0.27	0.27	0.22
Hematite	10.33	11.12	11.07	10.74	10.83	11.49	11.61	11.45	10.18
Trace element (ppm)									
Y	33	29	28	30	23	31	13	31	27
Ba	268	167	152	239	171	258	29	247	266
Cr	227	215	208	215	195	504	1214	518	514
V	190	208	207	202	236	221	198	223	194
Sc	32	32	33	33	37	33	38	36	36
Co	55	63	57	55	82	61	65	63	66
Ni	97	108	105	105	108	191	229	185	166
Cu	86	89	86	88	107	86	58	67	65
Zn	78	85	84	83	86	85	63	99	80
Ga	16	15	16	18	13	14	11	15	10
Pb	21	12	15	14	4	17	10	8	27
Th	6.5	8.3	7.6	6.2	3.0	6.9	1.2	8.5	7.4
Rb	93	48	40	64	22	49	1	45	45
U	0.4	0.4	0.5	0.4	0.4	0.4	0.1	0.4	0.4
Sr	141	129	163	150	183	152	65	135	124
Y	33	29	28	30	23	31	13	31	27
Zr	112	117	117	116	70	109	48	130	129
Nb	8	8	8	8	3	8	5	9	9
REE (ppm)									
La	18.12	9.33	12.83	7.09	4.00	15.31	6.47	17.54	6.49
Ce	37.24	21.15	30.73	14.44	9.89	35.34	14.12	37.34	14.47
Pr	4.47	2.37	3.31	1.89	1.14	3.90	1.80	4.29	1.94
Nd	16.16	8.56	11.99	6.70	4.37	14.27	6.92	15.64	6.92
Sm	3.39	1.88	2.80	1.43	1.04	3.10	1.74	3.24	1.40
Eu	0.89	0.45	0.68	0.35	0.34	0.75	0.52	0.71	0.27
Gd	3.61	2.03	2.78	1.53	1.17	3.33	1.97	3.47	1.51
Tb	0.55	0.29	0.43	0.22	0.18	0.51	0.33	0.53	0.20
Dy	3.43	1.77	2.26	1.33	1.16	3.02	2.09	3.13	1.16
Ho	0.73	0.39	0.57	0.27	0.25	0.66	0.43	0.67	0.23
Er	1.97	1.06	1.55	0.73	0.65	1.76	1.19	1.80	0.66
Tm	0.30	0.17	0.25	0.11	0.11	0.27	0.18	0.27	0.10

Table 2. *(Continued.)*

Sample #	SK13	SK14	SK16	SK17	SK18	SK20	SK21	SK31	SK37
Yb	1.99	1.04	1.64	0.75	0.69	1.79	1.15	1.76	0.71
Lu	0.33	0.18	0.26	0.12	0.11	0.28	0.17	0.29	0.11

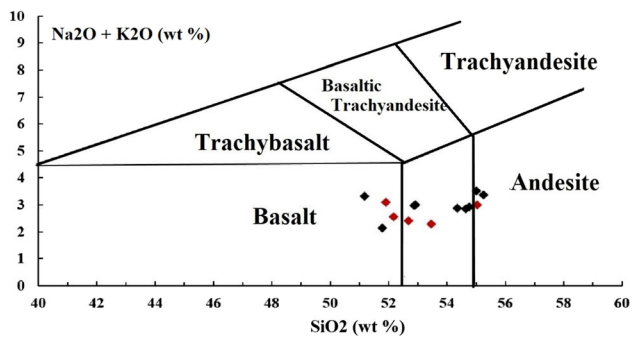

Figure 5. TAS plot of Khairagarh volcanics after Cox *et al.* (1979). Brown data points in plot taken from Khare and Asthana (2020). Khairagarh volcanics are sub-alkaline and plot in the fields of basalt, basaltic andesite to andesite.

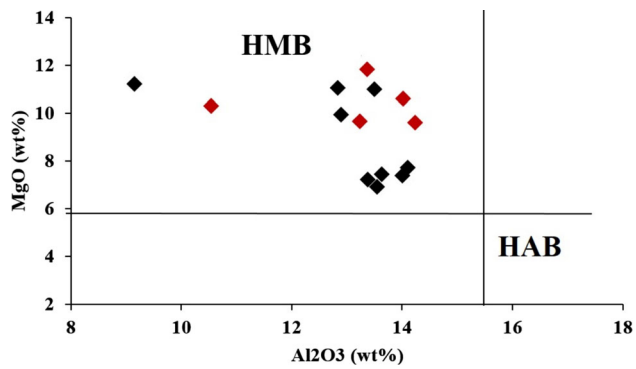

Figure 7. Al_2O_3 *vs.* MgO plot of Khairagarh volcanics after Kersting and Arculus (1994). Brown data points in the plot were taken from Khare and Asthana (2020). All samples plot in the field of high-Mg basalt.

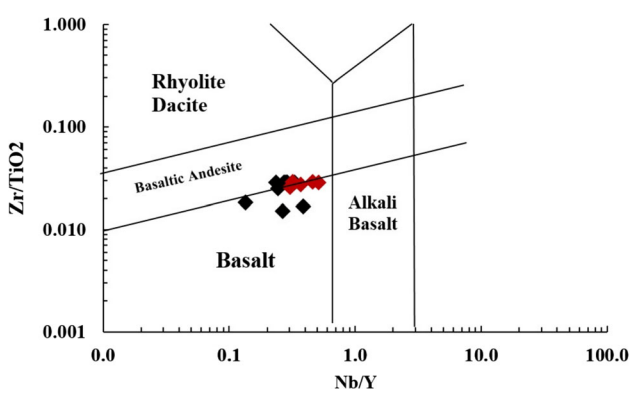

Figure 6. Nb/Y *vs.* Zr/TiO_2 plot of Khairagarh volcanics after Pearce (1996). Brown data points in the plot were taken from Khare and Asthana (2020). Khairagarh volcanics plot in the field of basalt and basaltic andesite.

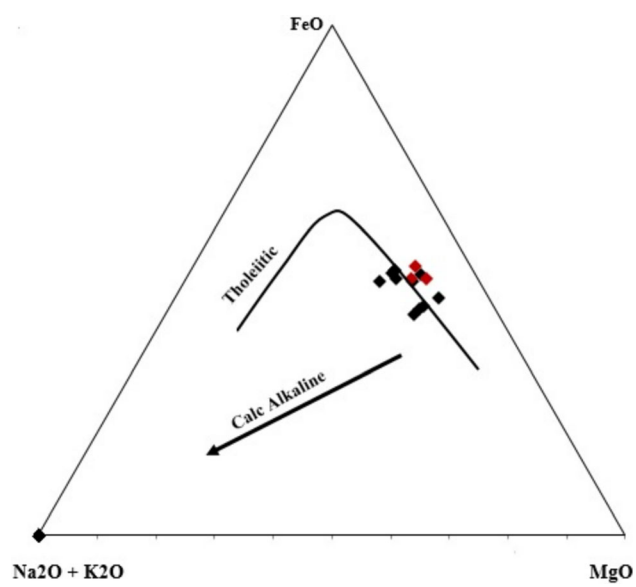

Figure 8. AFM plot of Khairagarh volcanics after Winchester and Floyd (1977). Volcanics show moderate iron enrichment tholeiitic trend. Brown data points in the plot were taken from Khare and Asthana (2020).

therefore, they give insights into the nature of mantle source. Table 3 presents HFSE ratios of Khairagarh volcanics, Fertile MORB Mantle (FMM), Primitive Upper Mantle (PUM), Enriched Upper Mantle (EUM) and Ocean Island Basalt (OIB) (c.f., McDonough and Sun 1995). Overall, HFSE ratios indicate mantle source with an elemental ratio close to PUM. CaO/TiO_2 ratios vary from 6 to 23, while Al_2O_3/TiO_2 vary from 15 to 22, which indicates a non-refractory fertile mantle source of Khairagarh volcanics.

7. Discussion

The beginning of the Proterozoic era in the northern Bastar Craton was marked with widespread Nandgaon bimodal volcanism, Dongargarh granite intrusion, followed by mafic magmatism in the Khairagarh basin. U–Pb dating by Manikyamba *et al.* (2016) has

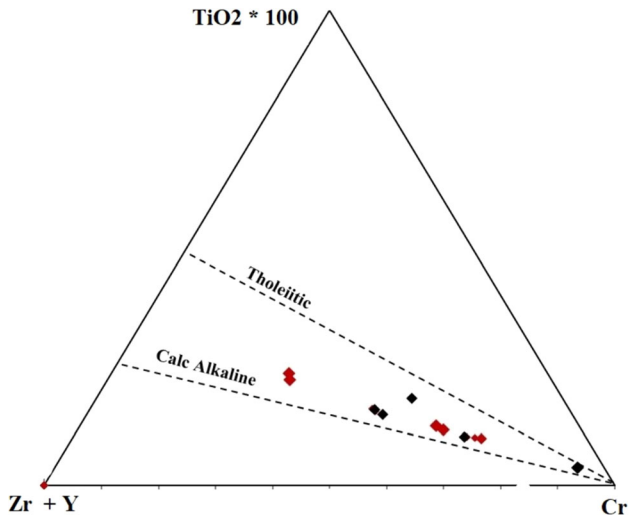

Figure 9. TYC plot of Khairagarh volcanics after Davies *et al.* (1979). Volcanics show an overall trend transitional between tholeiitic and calc-alkaline. Brown data points in the plot were taken from Khare and Asthana (2020).

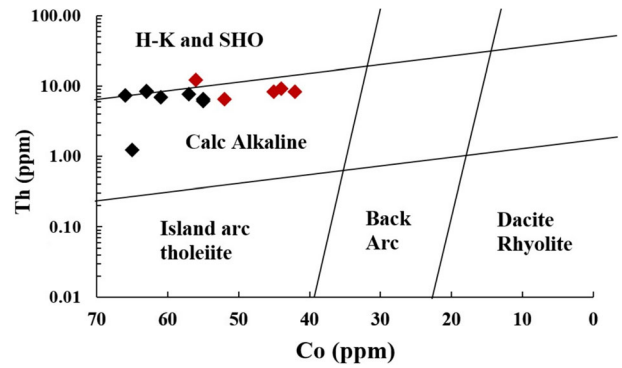

Figure 10. Co *vs.* Th plot of Khairagarh volcanics after Hastie *et al.* (2007). All samples plot in the field of calc-alkaline basalt. Brown data points in the plot were taken from Khare and Asthana (2020).

revealed near similar ages of Dongargarh granite (∼2.5 Ga) and Bijli rhyolite (∼2.48 Ga). U–Pb zircon geochronology by Khanna *et al.* (2019) has revealed the 2463 ± 45 Ma age of the Bortalao Formation, which marked the first phase of sedimentation in the Khairagarh basin. Bortalao Formation and its basement have near similar age, which indicates a major rapid crust formation event in northern Bastar Craton at around 2.4–2.5 Ga, which led to intrusion of Dongargarh granite, bimodal Bijli rhyolite volcanism and rifting of continental crust, resulting in formation of Khairagarh basin. U–Pb dating of Khairagarh sediments by Khanna *et al.* (2019) has revealed ∼2453 Ma age of Karutola sandstone and ∼2210 Ma age of Ghoghra sandstone, which indicates that sedimentation and volcanism in Khairagarh basin continued for around 243 million years.

7.1 *Tectonomagmatic model*

Our geochemical work reveals quartz normative, sub-alkaline, transitional to calc-alkaline, high-Mg basalt to basaltic andesite composition of Mangikhuta and Kotima volcanic formations. NMORB normalized incompatible element plots drawn for Khairagarh volcanic samples (figure 12) reveal negative anomaly of Nb with respect to Th, U and K_2O. Enrichment of LILE (K_2O, U, Th) and LREE (Ce, Nd, Sm) compared to HFSE of similar compatibility (Nb, Zr, Ti and Y) indicates enrichment of LILE and LREE in the mantle source of Khairagarh volcanics, which could be attributed to either fluid flux enrichment of the mantle source or to metasomatic and magma mixing processes. Slight enrichment of LREE with respect to HREE in REE plot (figure 11) can be attributed to both arc and continental rift setting. On Co *vs.* Th plot (figure 10), Khairagarh volcanics plot in calc-alkaline field indicating their genesis either in supra-subduction zone or due to magma mixing. On Zr *vs.* Ti plot (figure 13), Khairagarh volcanics plot in field of arc lava. However, on Ti *vs.* V plot (figure 14), Khairagarh volcanics plot in field transitional between arc and MORB. Ti/V in some samples is more than 20, which indicates their calc-alkaline character. From such contrasting geochemical signatures, we conclude that tectonomagmatic inferences solely drawn from geochemical data of volcanics can lead to misleading inferences, if not substantiated by field relations. Besides, tectonomagmatic models for the genesis of Phanerozoic igneous provinces cannot be superimposed on Archean Paleoproterozoic provinces. Several previous workers (Asthana *et al.* 1996; Neogi *et al.* 1996; Khanna *et al.* 2019) have inferred rift basin, back-arc basin to Andean type supra-subduction zone tectonic environment for Khairagarh Group. Neogi *et al.* (1996) inferred stable continental margin environment of Khairagarh sediments, which is distinct from trench/arc sediments. Field investigation of the Sitagota syncline reveals the presence of intertrappean ferruginous shales and thin Algoma-type BIF beds in Mangikhuta basalt, besides the presence of sulphide and oxide mineralization in volcanics. Such BIFs are chemically precipitated sediments with alternate thin layers of Fe minerals and chert (Gourcerol *et al.* 2016). Local deposition of

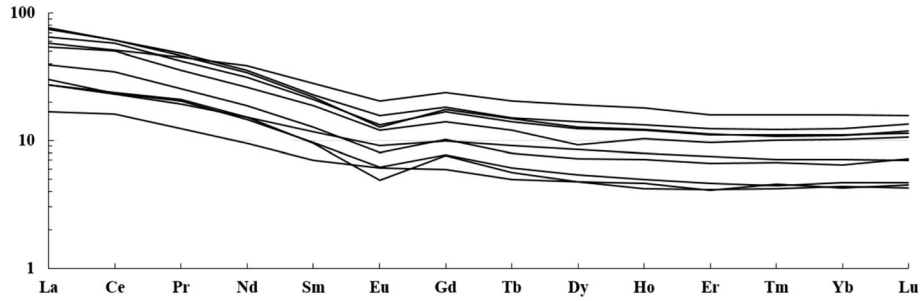

Figure 11. Chondrite normalized REE plot of Khairagarh volcanics with normalization values taken from McDonough and Sun (1995). Mild enrichment of LREE and negative Eu anomaly seen in the plot.

Table 3. *HFSE ratios of Khairagarh volcanics compared with HFSE ratios of fertile MORB mantle (FMM), Primitive Upper Mantle (PUM), Enriched MORB (EMORB) and Ocean Island Basalts (OIB). The HFSE values taken from McDonough and Sun (1995).*

Element ratio	FMM	PUM	EMORB	OIB	Current study	Khare and Asthana (2020)	Khanna *et al.* (2019)
Zr/Nb	32	16	9	6	10–23	11–15	16–17
Ti/Zr	130	116	82	61	34–60	34–39	43–54
Ti/V	13	15	40		15–23	19–22	14–33
Zr/Y	2.6	2.5	3.3	97	3–6	5–6	5–6

Algoma-type BIF is a common feature of Eoarchean Paleoproterozoic volcano-sedimentary sequences in greenstone belts. Such a BIF deposition model corresponds to semi-closed Khairagarh basin with extensive volcanism and hydrothermal fluids (c.f. Bekker *et al.* 2010; Gourcerol *et al.* 2016). Radiating mafic dyke swarms reported in this area have geochemical and geochronological similarities with the Khairagarh volcanics. Such dykes indicate a rift rather than subduction zone tectonic environment for Khairagarh basin. Therefore, based on geochronology, field geological and geochemical data, we infer rifting in stable continental crust led to the genesis of the Khairagarh basin, which led to the deposition of continent-derived sediments and massive mafic magmatism (figure 15a). The presence of calc-alkaline and quartz normative composition of Khairagarh volcanics is consistent with an evolved or late stages of a continental rift. Arc-related geochemical signatures of Khairagarh mafics could be due to its spatial and temporal proximity to Dongargarh Kotri mobile belt, which some workers infer as a paleo subduction zone. From a modern plate tectonics perspective, the rapid opening of stable continental crust along a continental margin could be due to the formation of a back-arc basin, although the nature of plate tectonics, size of plates, and prevailing geothermal gradients in Archean Proterozoic times vis-a-vis Phanerozoic are little understood.

7.2 *Post emplacement deformation*

Our current and previous work reveals the ubiquitous presence of chlorite, zoisite, prehnite, and pumpellyite mineral aggregates in Khairagarh volcanics, which, along with the absence of schistosity and foliations in them, indicates their very low-grade regional metamorphism. Previous work by Patel *et al.* (2008) and Khanna *et al.* (2019) has established alteration and very low-grade metamorphism of Khairagarh volcanics. However, field investigation and regional structures inferred from DEM indicate several phases of orogeny undergone by volcano-sedimentary succession post its deposition in the Khairagarh basin. Khairagarh sediments gradually mature from the lower Bortalao to the upper Karutola and Ghoghra formations. The lower Bortalao Formation consists of conglomerates, arenites, arkosic sandstone, arenites, upper conglomerates, and tuffaceous sandstones (Sarkar 1957, 1994) whereas upper Karutola and Ghoghra sandstone formations consist of quartz arenite and sub-arkosic arenite (Chakraborty and Sensarma 2008; Khanna *et al.* 2019). Sarkar *et al.* (1994) and Sensarma (2007, 2011) reported relation of Mangikhuta and Sitagota volcanics through fractionation, although several previous workers (Sarkar 1957; Rao *et al.* 1981; Longjam and Talat 2012) classified each volcanic unit as a separate lithostratigraphic unit. Sensarma and Mukhopadhyay (2014) reported the absence of any discordance between the volcanic and

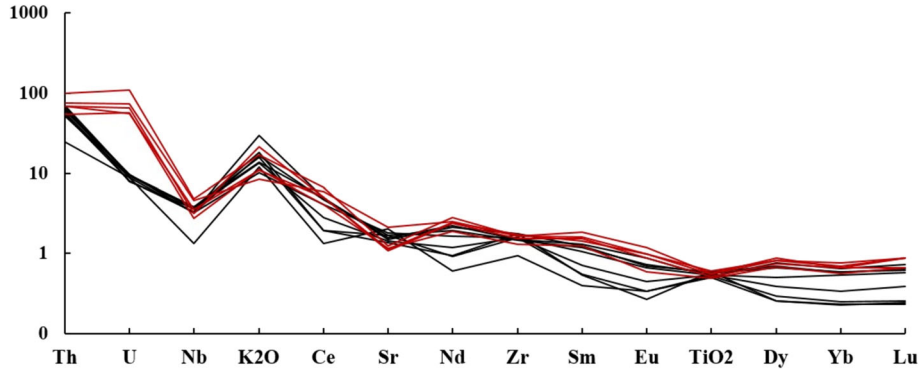

Figure 12. NMORB normalized incompatible element plot of Khairagarh volcanics. Th and U are enriched with respect to Nb. Ce is enriched with respect to Sr. Ti is depleted with respect to elements of similar compatibility. Normalization values are taken from Pearce and Parkinson (1993). Brown curves are plotted from Khare and Asthana (2020).

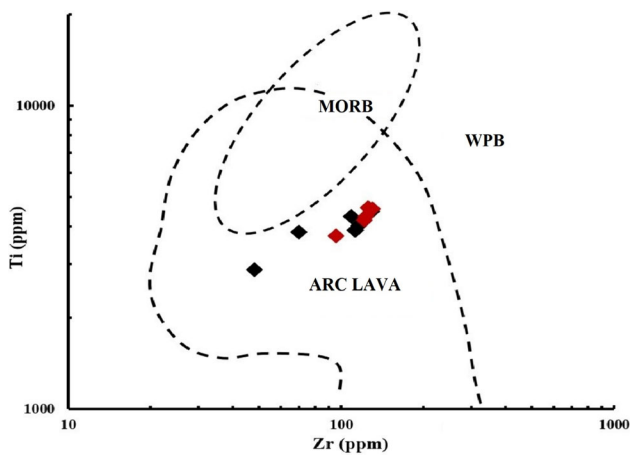

Figure 13. Khairgarh volcanics plotted on Zr *vs.* Ti plot after Pearce (1982). Ti shows coherent increasing trend with fractionation. All samples plot in the field of arc lava. Brown data points in plot taken from Khare and Asthana (2020).

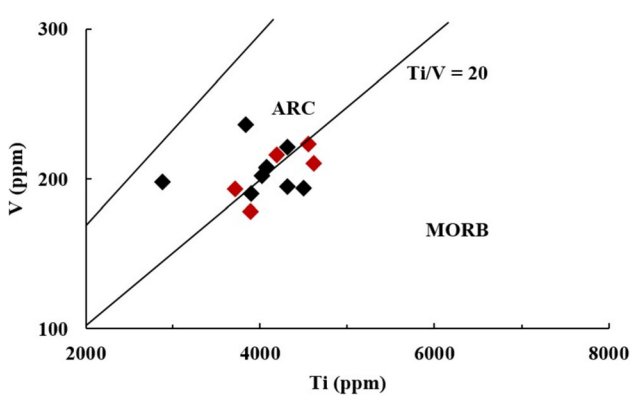

Figure 14. Ti *vs.* V plot of Khairagarh volcanics after Shervais (1982). Brown data points in plot taken from Khare and Asthana (2020).

sedimentary formations of the Khairagarh Group. Khanna *et al.* (2019) inferred that Khairagarh volcanics formed in a few tens of million years, although no geochronology data exists for Khairagarh volcanics. Our previous relict clinopyroxenes chemistry study (Khare and Asthana 2020; Khare *et al.* 2022) indicates the formation of Mangikhuta high-Mg andesite from fractionation of Kotima high Mg-basalt, which supports the findings of Khanna *et al.* (2019). It also validates the findings of Sensarma and Mukhopadhyay (2014) that volcanic are related by fractionation. With this perspective, we present a tectonomagmatic model (figure 15) for the genesis of Khairagarh volcano-sedimentary basin. This model proposes rapid opening and closure of continental crust in the northern Bastar Craton from ∼2.46 to 2.2 Ga. EW trending extension tectonics and rifting in the northern portion of Bastar Craton around 2.46 Ga led to the formation of the Khairagarh basin in which Bortalao sediments were deposited near the shore, whereas Karutola and Ghoghra sediments were deposited away from the shore (figure 15a). The Bortalao and Karutola sediments give overlapping U–Pb zircon ages (around 2.51–2.4 Ga and 2.48–2.4 Ga, respectively). The sediments were derived from a continental basement made of mafic and felsic rocks (Sarkar 1957, 1994; Sensarma and Mukhopadhyay 2014). Magmatism from the centre of the basin led to the deposition of primitive Kotima basalt towards the centre and fractionated Mangikhuta basaltic andesite towards the shore (c.f. Khare and Asthana 2020; Khare *et al.* 2022). The discordance between sediments and volcanics is not reported by any worker. Rifting in continental crust was followed by volcanism and sedimentation. Later onset of EW compression led to the closure of the Khairagarh basin (figure 15b). We correlate this opening and closure of Khairagarh basin to a NS trending Paleoproterozoic Dongargarh Kotri mobile

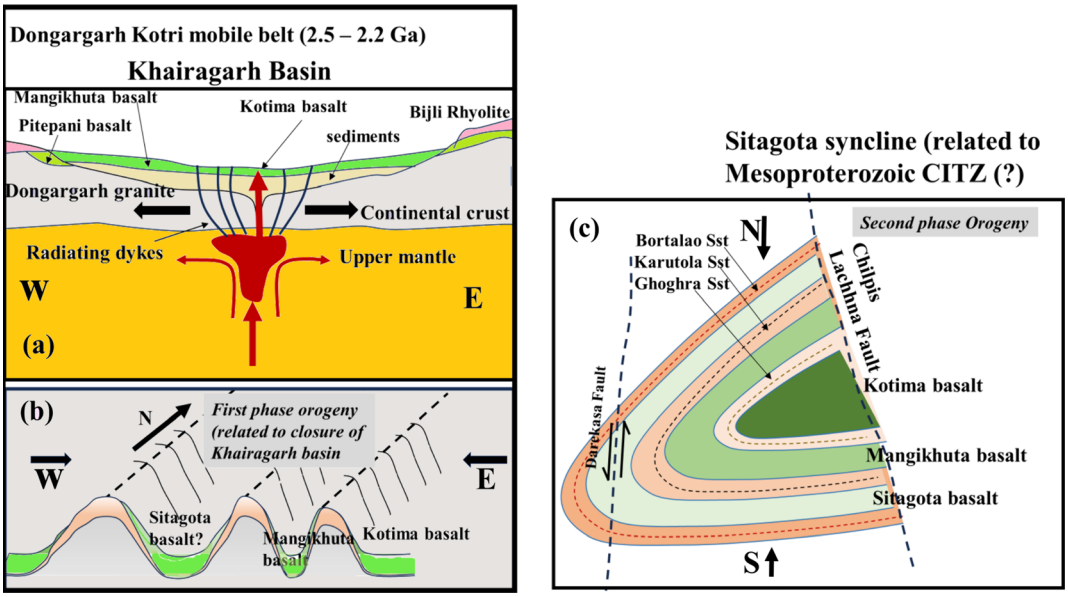

Figure 15. Tectonomagmatic model of Khairagarh basin illustrating (**a**) rifting, sedimentation, magmatism and formation of radiating dykes, (**b**) closure of Khairagarh basin due to EW compressive forces of Dongargarh Kotri mobile belt and (**c**) formation of regional Sitagota syncline structure due to Mesoproterozoic central Indian tectonic zone (CITZ).

belt in the Bastar Craton (c.f. Ramakrishnan and Vaidyanathan 2010). Later, the second phase NS trending compressive regime led to the formation of NE–SW trending Sitagota syncline with the previous generation folds forming its two limbs (figure 15c). The second phase compression led to the deformation and development of 12 major NS trending faults affecting the limbs and hinges of the syncline (Sarkar 1957). The NS trending Darekasa fault in the western limb of syncline (Sarkar 1957) and another prominent NS trending Lachhna fault towards the east of syncline indicate a regional NS compressive force operating in northern Bastar Craton, which was probably due to the collision of north Bastar Craton with Bundelkhand Craton manifested as a prominent EW trending Mesoproterozoic Central Indian Suture Zone (Yedekar *et al.* 1990; Acharyya 2003). Ghosh *et al.* (2006) performed microstructural analyses and grain-scale measurements of Sitagota syncline sediments and reported two sets of cleavage fabrics peculiar to a low-grade low-strain belts. The ubiquitous presence of very low-grade metamorphic mineral assemblages (prehnite, pumpellyite, chlorite) in Khairagarh volcanics indicates that the Mangikhuta, Kotima and lower Sitagota volcanic formations did not undergo high P–T transformation, and the alteration and very low-grade metamorphism took place at near surface conditions.

7.3 *Global implications*

Previous workers (Rogers and Santosh 2003; Longjam and Talat 2012) relate Paleoproterozoic rapid crustal growth of Bastar Craton to its association with Ur supercontinent. However, paleomagnetic dyke swarm data of neighbouring Singhbhum Craton in the Indian shield indicates its ancestry to Vaalbara supercontinent (Kumar *et al.* 2017). Rifting and mafic magmatism similar to Khairagarh basin is reported from coeval Lower Wyloo Group in Pilbara Craton and Hekpoort and Ongeluk basalt formations of Transvaal basin in Kaapvaal Craton (Eglington and Armstrong 2004; Humbert *et al.* 2018, 2020), which constitute Vaalbara supercontinent. Therefore, we propose areal extent of Vaalbara supercontinent (de Kock *et al.* 2009; Smirnov *et al.* 2013; Kampmann *et al.* 2015; Kumar *et al.* 2017) from Kaapvaal Craton in south Africa through Bastar Craton and Singhbhum Craton in Indian shield to Pilbara Craton in Australia in the Neoarchean Paleoproterozoic (2.8–2.1 Ga) times.

8. Conclusion

The following conclusions are drawn from the geological study of Khairagarh Group rocks in Sitagota syncline.

1. The volcanic rocks towards centre of syncline are sub-alkaline, low-Ti, high-Mg basalt to basaltic andesite with geochemical characteristics varying from tholeiitic, transitional to calc-alkaline. The mantle source of volcanics was enriched to primitive upper mantle.
2. Fe-oxide and Cu-sulphide mineralization is reported in Mangikhuta basalt formation of Khairagarh Group. Intertrappean shale and Algoma-type BIF beds are present in this volcanic formation. Tectonomagmatic model indicates rifting of stable continental crust led to sedimentation, massive mafic magmatism, and genesis of Khairagarh Group.
3. The Sitagota syncline is elevated towards the centre with a maximum elevation of around 800 m. The Khairagarh basin underwent EW and NS compression and orogeny probably related to Paleoproterozoic DKMB and Mesoproterozoic CITZ, respectively. NS compression led to the genesis of sinistral NS trending Lachhna, Borla and Darekasa faults. However, Khairagarh volcanic formations did not undergo high P–T transformation and most of the alteration and very low-grade metamorphism took place at near surface conditions.
4. The areal extent of Vaalbara supercontinent extended from Kaapvaal Craton in south Africa through Bastar Craton and Singhbhum Craton in Indian shield to Pilbara Craton in Australia in the Neoarchean Paleoproterozoic (2.8–2.1 Ga) times.

Acknowledgements

Authors thank DST SERB grant CRG/2022/004833 and UPES Dehradun for funding this research. Authors thank the Wadia Institute of Himalayan Geology (WIHG), Dehradun, for the geochemical analysis of rock samples. Authors thank Dr Ashish Agarwal from UPES, Dehradun for preparation of digital elevation map of syncline on ArcGIS. Authors thank Dr Girish Kothyari, UPES for digitizing the geological map of Sitagota syncline. Authors thank Dr A K Singh, WIHG, for the critical review of the manuscript and for providing suggestions that led to the improvement of contents. The authors are grateful to Dr Talat Ahmad for the critical review of the manuscript, which led to the refining of the contents. Funding: Science and Engineering Research grant/Award No CRG/2022/004833 and UPES SEED Grant/Award 2021.

Author statement

Sunil Kumar Khare: Conceptualization, data curation, fieldwork, formal analysis, writing – original draft, interpretation. D Asthana: Fieldwork and interpretation. A S Venkatesh: Petrography, fieldwork and interpretation.

References

Acharyya S K 2003 The nature of Mesoproterozoic Central Indian Tectonic Zone with exhumed and reworked older granulites; *Gondwana Res.* **6(2)** 197–214.

Anhaeusser C R 2014 Archaean greenstone belts and associated granitic rocks – A review; *J. Afr. Earth Sci.* **100** 684–732.

Arndt N T 1986 Spinifex and swirling olivines in a Komatiite lave lake. Munro township, Canada; *Precamb. Res.* **34** 139–155.

Arya D, Gupta S, Kumar S and Xu X 2021 Geochemistry and U-Pb-Lu-Hf zircon isotopes of Cu ± Au ± Mo hosted granitoids of Malanjkhand pluton, Central India: Implications on petrogenesis, source, and crustal evolution; *Lithos* **402–403** 106151.

Asthana D, Dash M R, Pophare A M and Khare S K 1996 Interstratified low-high Ti volcanics from arc-related Khairagarh Group of Central India; *Curr. Sci.* **71** 304–306.

Asthana D, Khare S K, Pophare A M and Dash M R 1997 Comments on "Geochemistry of the Dongargarh volcanic rocks, Central India: Implications for the Precambrian mantle"; *Precamb. Res.* **84** 105–107.

Asthana D, Dash M R, Khare S K and Pophare A M 2001 Paleoproterozoic Hi–Mg Andesite and related igneous rocks from Central India and their geodynamic implications; *Gondwana Res.* **4(4)** 565–566.

Bekker A, Slack J F, Planavsky N, Krapez B, Hofmann A, Konhauser K O and Rouxel O J 2010 Iron formation: The sedimentary product of a complex interplay among mantle, tectonic, oceanic, and biospheric processes; *Econ. Geol.* **105** 467–508.

Cawood P A, Hawkesworth C J, Pisarevsky S A, Dhuime B, Capitanio F A and Nebel O 2018 Geological archive of the onset of plate tectonics; *Phil. Trans. Roy. Soc. Am.* **376** 20170405.

Chakraborty T and Sensarma S 2008 Shallow marine and coastal eolian quartz arenites in the Neoarchean-Palaeoproterozoic Karutola Formation, Dongargarh Volcano-sedimentary succession, central India; *Precamb. Res.* **162(1–2)** 284–301.

Chalapathi Rao N V and Srivastava R K 2009 A new find of Boninite dyke from the Paleoproterozoic Dongargarh Supergroup: Inference for a fossil subduction zone in the Archaean of the Bastar Craton, Central India; *Neues Jahrbuch Für Min. Abhandlungen* **186(3)** 271–282.

Codillo E A, Le Roux V and Marschall H R 2018 Arc-like magmas generated by mélange-peridotite interaction in the mantle wedge; *Nat. Commun.* **9** 2864.

Condie K C and Kroner A 2008 When did plate tectonics begin? Evidence from Geologic record; *Geol. Soc. Am. Spec. Paper* **440** 1–14.

Cox K G, Bell J D and Pankhurst R J 1979 *The interpretation of igneous rocks*; George Allen and Unwin, London.

Davies F J, Grant R W E and Whitehead R E S 1979 Immobile trace elements and Archaean volcanic stratigraphy in the Timmins mining area, Ontario; *Can. J. Earth Sci.* **16** 305–311.

Deb G K, Saha D, Deb S P and Banerjee A 2021 Coexisting arc and MORB signatures in the Sonakhan greenstone belt, India: Late Neoarchean–early Proterozoic subduction roll-back and back-arc formation; *Am. J. Sci.* **321(9)** 1308–1349.

de Kock M O, Evans D A D and Beukes N J 2009 Validating the existence of Vaalbara in the Neoarchean; *Precamb. Res.* **174(1–2)** 145–154.

Eglington B M and Armstrong R A 2004 The Kaapvaal Craton and adjacent orogens, southern Africa: A geochronological database and overview of the geological development of the craton; *S. Afr. J. Earth Sci.* **107** 13–32.

Elliot T, Plank T O, Zindler A, White W and Bourdon B 1997 Element transport from slab to volcanic front at the Mariana Arc; *J. Geophys. Res.* **102(B7)** 14,991–15,019.

Ewart A, Collerson K D, Regelous M, Wendt J I and Niu Y 1998 Geochemical evolution within the Tonga Kermadec Lau Arc Back Arc systems: The role of varying mantle wedge composition in time and space; *J. Petrol.* **39** 331–368.

Foley B 2022 Generation of Archean TTGs by slab melting during sluggish, drip-like subduction. EGU Vienna, 23–27 May, 2022EGUGA.2410873F.

Gaetani G A, Grove T L and Bryan W B 1993 The influence of water on the petrogenesis of subduction related igneous rocks; *Nature* **365** 332–334.

Ghosh G, Chakraborty S, Mukhopadhyay J and Ray A 2006 Grain-scale deformation in the Paleoproterozoic Dongargarh Supergroup, central India: Implications for shallow crustal deformation mechanisms from microstructural analysis; *Geol. Mag.* **143** 531–543.

Gourcerol B, Thurston P C, Kontak D J, Côté-Mantha O and Biczok J 2016 Depositional setting of Algoma-type banded iron formation; *Precamb. Res.* **281** 47–79.

Hastie A R, Kerr A C, Pearce J A and Mitchell S F 2007 Classification of altered volcanic island arcs rocks using immobile trace elements: Development of Th–Co discrimination diagram; *J. Petrol.* **48** 2341–2357.

Hawkesworth C J and Brown M 2018 Earth dynamics and the development of plate tectonics; *Phil. Trans. Roy. Soc.* **A376** 20180228.

Hawkesworth C J, Gallagher K, Hergt J M and McDermott F 1994 Destructive plate margin magmatism: Geochemistry and melt generation; *Lithos* **33** 169–188.

Humbert F, de Kock M, Altermann W, Elburg M A, Lenhardt N and Smith A J B 2018 Petrology, physical volcanology and geochemistry of a Paleoproterozoic large igneous province: The Hekpoort Formation in the southern Transvaal subbasin (Kaapvaal craton); *Precamb. Res.* **315** 232–256.

Humbert F, Agangic A, Massuyeauc M, Elburgc M A, Belyaninc G, Smith A J B, Laccherie L M, Coetzeea L L and Waboc H 2020 Rifting of the Kaapvaal Craton during the early Paleoproterozoic: Evidence from magmatism in the western Transvaal subbasin (South Africa); *Precamb. Res.* **342** 1–22.

Kamber B S 2015 The evolving nature of terrestrial crust from the Hadean, through the Archaean, into the Proterozoic; *Precamb. Res.* **258** 48–82.

Kampmann T C, Gumsley A P, de Kock M O and Söderlund U 2015 U–Pb geochronology and paleomagnetism of the Westerberg Sill Suite, Kaapvaal Craton – support for a coherent Kaapvaal–Pilbara Block (Vaalbara) into the Paleoproterozoic?; *Precamb. Res.* **269** 58–72.

Keleman P B 1995 Genesis of high Mg# Andesites and the continental crust; *Contrib. Mineral. Petrol.* **120** 1–19.

Kelley K A, Plank T, Newman S, Edward M S, Grove T L, Parman S and Erik H H 2010 Mantle melting as a function of water content beneath the Mariana Arc; *J. Petrol.* **51** 1711–1738, https://doi.org/10.1093/petrology/egq036.

Kersting A B and Arculus R J 1994 Klyuchevskoy Volcano, Kamchatka, Russia: The role of high-flux recharged, tapped, and fractionated Magma Chamber(s) in the genesis of high-Al_2O_3 from high-MgO basalt; *J. Petrol.* **35** 1–41.

Khanna P P, Saini N K, Mukherjee P K and Purohit K K 2009 An appraisal of ICP–MS technique for determination of REEs: Long term QC assessment of silicate rock analysis; *Him. Geol.* **30** 95–99.

Khanna T C, Bizimis M, Barbeau D I, Krishna A K and Sesha Sai V V 2019 Evolution of ca. 2.5 Ga Dongargarh volcano-sedimentary Supergroup Bastar Craton Central India: Constraints from zircon U–Pb geochronology bulk rock geochemistry and Hf–Nd isotope systematics; *Earth Sci. Rev.* **190** 273–309.

Khare S K and Asthana D 2020 Petrogenesis of Neoarchean Mangikhuta Volcanics Complex Dongargarh Supergroup Central India: Insights from relict clinopyroxene chemistry; *J. Geol. Soc. India* **96** 363–373.

Khare S K, Asthana D and Venkatesh A S 2022 Petrogenetic insights from relict augites in Neoarchean Kotima basalt of Dongargarh Supergroup, Bastar Craton, Central India; *J. Earth Syst. Sci.* **131** 1–22, https://doi.org/10.1007/s12040-021-01747-3.

Khare S K, Shukla A D and Venkatesh A S 2024 Vanadium rich Fe-Ti oxide and Cu-sulphide mineralization in Paleoproterozoic Mangikhuta volcanics, Central Indian Craton: Metallogenic and petrogenetic implications; *Ore Energy Resour. Geol.* **16** 100041, ISSN 2666-2612, https://doi.org/10.1016/j.oreoa.2024.100041.

Krishnamurthy P 2014 Back to basics: Exploration strategies for Uranium in the Dongargarh Supergroup (DSG), Central India; In: National Workshop on "Recent Advances in Geology of Dongargarh-Kotri Belt, Central India and its Mineral Potential", 21–22 June 2012, Nagpur.

Krishnamurthy P, Sinha D K, Rai A K, Seth D K and Singh S N 1990 Magmatic rocks of the Dongargarh Supergroup, Central India. Their petrological evolution and implications on metallogeny; *GSI Spec. Publ.* **28** 303–319.

Kumar H and Asthana D 2018 The 2.5 Ga Malanjkhand Cu deposit of Central India; *J. Indian Sci. Cong.* **9** 5–24.

Kumar S and Rino V 2006 Mineralogy and geochemistry of micro granular enclaves in Paleoproterozoic Malanjkhand

granitoids, central India: Evidence of magma mixing, mingling, and chemical equilibration; *Contrib. Mineral. Petrol.* **152** 591–609, https://doi.org/10.1007/s00410-006-0122-3.

Kumar A, Parashuramulu V, Shankar R and Besse J 2017 Evidence for a Neoarchean LIP in the Singhbhum Craton, eastern India: Implications to Vaalbara supercontinent; *Precamb. Res.* **292** 163–174.

Kuritani T, Yoshida T, Kimura J I, Hirahara Y and Takahashi T 2014 Water content of primitive low-K tholeiitic basalt magma from Iwate Volcano, NE Japan arc: Implications for differentiation mechanism of frontal-arc basalt magmas; *Mineral. Petrol.* **108** 1–11, https://doi.org/10.1007/s00710-013-0278-2.

Li H Y, Li X, Ryan J G, Zhang C and Xu Y G 2022 Boron isotopes in Boninite document rapid changes in slab inputs during subduction initiation; *Nat. Commun.* **13** 993, https://doi.org/10.1038/s41467-022-28637-6.

Longjam K C and Talat A 2012 Geochemical characterization and petrogenesis of Proterozoic Khairagarh volcanics: Implication for Precambrian crustal evolution; *Geol. J.* **47** 130–143.

Lowrey J R, Ivanic T J, Wyman D A and Robert M P 2017 Platy Pyroxene: New insights into Spinifex texture; *J. Petrol.* **58** 1671–1700, https://doi.org/10.1093/petrology/egx069.

Manikyamba C, Santosh M, Chandan K B, Rambabu S, Li T, Saha A, Arubam C K, Ganguly S, Singh D and Subba Rao D V 2016 Zircon U–Pb geochronology, Lu–Hf isotope systematics, and geochemistry of bimodal volcanic rocks and associated granitoids from Kotri Belt, Central India: Implications for Neoarchean–Neoarchean crustal growth; *Gondwana Res.* **38** 313–333.

Martin H 1986 Effect of steeper Archean geothermal gradient on geochemistry of subduction-zone magmas; *Geology* **14** 753–756.

McDonough W F and Sun S S 1995 The composition of the Earth; *Chem. Geol.* **120** 223–253.

Mohanty S 2015 Paleoproterozoic supracrustals of Bhandara craton: Dongargarh Supergroup and Sausar Group; *Geol. Soc. London, Memoir,* https://doi.org/10.1144/M43.11.

Mondal M E A, Faruquie M H and Ahmad T 2006 Continental Growth of Bhandara Craton, Central Indian Shield during Precambrian via multiphase subduction and lithospheric extension/rifting: Evidence from geochemistry of gneisses, granitoids and mafic dykes; *J. Geosci., Osaka City Univ.* **49** 137–151.

Murton B J 1989 Tectonic controls on Boninite genesis; *Geol. Soc. London, Spec. Publ.* **42** 347–377.

Naqvi S M and Rogers J W 1987 *Precambrian geology of India*; Cambridge Univ. Press.

Nehru C and Sikka D B 2014 Mafic dikes and dike swarms from the Dongargarh-Kotri Belt: With special reference to Malanjkhand Porphyry, Copper nearby areas and mine; In: National Workshop on "Recent Advances in Geology of Dongargarh-Kotri Belt, Central India and its Mineral Potential", 21–22 June 2012, Nagpur.

Neogi S, Miura H and Hariya Y 1996 Geochemistry of Dongargarh volcanics rocks Central India: Implications for the Precambrian mantle; *Precamb. Res.* **76** 77–91.

Pandit D and Panigrahi M K 2012 Comparative petrogenesis and tectonics of Paleoproterozoic Malanjkhand and Dongargarh granitoids, Central India; *J. Asian Earth Sci.* **50** 14–26.

Pandit D, Panigrahi M K, Moriyama T and Ishihara S 2014 Comparative geochemical, magnetic susceptibility, and fluid inclusion studies on the Paleoproterozoic Malanjkhand and Dongargarh granitoids, Central India and implications to metallogeny; *Mineral. Petrol.* **108** 663–680.

Panigrahi M K, Bream B R, Misra K C and Naik R K 2004 Age of granitic activity associated with copper–molybdenum mineralization at Malanjkhand, Central India; *Miner. Depos.* **39** 670–677.

Patel S C, Asthana D and Acharya C S 2008 Prehnite and Pumpelleyite in the Archaean Sitagota Volcanics near Deori, Bhandara District, Maharashtra; *J. Geol. Soc. India* **72(2)** 208–212.

Peacock S M, Rushmer T and Thompson A B 1994 Partial melting of subducting oceanic crust; *Earth Planet. Sci. Lett.* **121** 227–244.

Pearce J A 1982 Trace element characteristics of lavas from destructive plate boundaries; In: *Andesites* (ed.) Thorpe R S, John Wiley.

Pearce J A 1996 User guide to Basalt discriminant diagram; In: Trace element geochemistry of volcanic rocks, Applications for massive sulphide exploration (ed.) Wyman D A, *Geol. Assoc. Can.* **12** 79–113.

Pearce J A and Cann J R 1973 Tectonic setting of basic volcanic rocks determined using trace element analyses; *Earth Planet. Sci. Lett.* **19** 290–300.

Pearce J A and Parkinson I J 1993 Trace element models for mantle melting: Application to volcanic arc petrogenesis; In: Magmatic processes and plate tectonics, *Geol. Soc. Spec. Publ.* **76** 373–403.

Pearce J A and Peate D W 1995 Tectonic implications of composition of volcanic arc magmas; *Ann. Rev. Earth Planet. Sci.* **23** 251–285.

Peate D W, Pearce J A, Hawkesworth C J, Colley H, Edwards C M H and Hirose K 1997 Geochemical variation in Vanuatu arc lavas: The role of subducted material and a variable mantle wedge composition; *J. Petrol.* **38** 1331–1358.

Radhakrishna B P and Naqvi S M 1986 Precambrian continental crust of India and its evolution; *J. Geol.* **94** 145–166.

Rajesh H M, Chisonga B C, Shindo K, Beukes N K and Armstrong R A 2013 Petrographic, geochemical and SHRIMP U-Pb titanite age characterization of the Thabazimbi mafic sills: Extended time frame and a unifying petrogenetic model for the Bushveld Large Igneous Province; *Precamb. Res.* **230** 79–102.

Ramakrishnan M and Vaidyanathan R 2010 Geology of India; 1157, **1** Geol. Soc. India, Bangalore.

Rao G V 1981 The correlation of Dongargarh Chilpi and Sausar Groups; *GSI Spec. Publ.* **3** 9–15.

Regelous M, Collerson K, Ewart A and Wendt J I 1997 Trace element transport rates in subduction zones: Evidence from Th, Sr and Pb isotope data for Tonga-Kermadec arc lavas; *Earth Planet. Sci. Lett.* **150** 291–302.

Rogers J J W and Santosh M 2003 Supercontinents in Earth history; *Gondwana Res.* **6(3)** 357–368.

Saini N K, Mukherjee P K, Rathi M S and Khanna P P 2000 Evaluation of energy dispersive X-ray fluorescence

spectrometry in the rapid analysis of silicate rocks using pressed powder pellets; *X-Ray Spectrometry* **29** 166–172.

Santosh M, Tsunogae T, Yang C, Han Y, Hari K R, Prasanth M P M and Uthup S 2020 The Bastar Craton central India: A window to Archean–Paleoproterozoic crustal evolution; *Gondwana Res.* **79** 157–184.

Sarkar S N 1957, 1958 Stratigraphy and tectonics of Dongargarh System: A new system in the Precambrian of Bhandara-Durg Balaghat area Bombay and MP; *J. Sci. Eng. Res.* **1** 237–268.

Sarkar S N 1994 Chrono stratigraphy and tectonics of the Dongargarh Supergroup Precambrian rocks in Bhandara-Durg region, Central India; *Ind. J. Earth Sci.* **21** 19–31.

Sarkar S N, Gopalan K and Trivedi J R 1981 New data on the geochronology of the Precambrians of Bhandara-Drug, central India; *Indian J. Earth Sci.* **8** 131–151.

Sarkar S N, Sarkar S S and Ray S L 1994 Geochemistry and genesis of the Dongargarh Supergroup Precambrian rocks in Bhandara-Durg Region Central India; *Ind. J. Earth Sci.* **21** 117–126.

Sensarma S 2007 A bimodal large igneous province and the plume debate: The Paleoproterozoic Dongargarh group, central India; *Geol. Soc. Am. Spec. Paper* **430** 831–839.

Sensarma S 2011 Geodynamic processes at the Neoarchaean-Palaeoproterozoic transition in the Bastar craton: Insight from the Dongargarh volcanic-sedimentary sequence; *Indian J. Geosci.* **65(2)** 88–96.

Sensarma S and Mukhopadhyay D 2014 Stratigraphy of ∼2.5 Ga Dongargarh Belt Central India: Key observations and suggested revisions; *Gondwana Geol. Mag.* **16** 41–48.

Shaw D M 1970 Trace element fractionation during anataxis; *Geochim. Cosmochim. Acta* **34** 237–243.

Shervais J W 1982 Ti–V plots and the petrogenesis of modern and ophiolitic lavas; *Earth Planet. Sci. Lett.* **59(1)** 101–118.

Sikka D B and Nehru C 1997 Review of Precambrian Porphyry Cu±Mo±Au deposits with special reference to Malanjkhand porphyry copper deposit, India; *J. Geol. Soc. India* **49** 239–288.

Sinha D K, Das L K, Dash J K, Singh A, Majumdar A, Goswami S and Kumar A 2014 Mapping subsurface structures beneath the Bodal and Bhandaritola Uranium Prospects, Dongargarh–Kotri Belt Central India: Insights from the detailed gravity, magnetic, resistivity and induced polarization/resistivity gradient survey; In: National Workshop on "Recent Advances in Geology of Dongargarh–Kotri Belt, Central India and its Mineral Potential", 21–22 June 2012, Nagpur.

Smirnov A V, Evans D A D, Ernst R E, Söderlund U and Zheng-Xiang Li 2013 Trading partners: Tectonic ancestry of southern Africa and western Australia, in Archean supercratons Vaalbara and Zimgarn, *Precamb. Res.* **224** 11–22.

Sridhar M, Chaturvedi A K, Rai A K and Parihar P S 2014 Airborne geophysical surveys for mineral exploration in Kotri–Dongargarh Rift Zone, Central India; In: National Workshop on "Recent Advances in Geology of Dongargarh–Kotri Belt, Central India and its mineral potential", 21–22 June 2012, Nagpur.

Srivastava R K and Gautam G C 2009 Precambrian mafic magmatism in the Bastar Craton, Central India; *J. Geol. Soc. India* **72** 52–72.

Tatsumi Y 2000 Slab melting: Its role in continental crust formation and mantle evolution; *Geophys. Res. Lett.* **27** 3941–3944.

Tatsumi Y and Hanyu H 2003 Geochemical modeling of dehydration and partial melting of subducting lithosphere: Toward a comprehensive understanding of high-Mg andesite formation in the Setouchi volcanic belt, SW Japan; *Geochem. Geophys.* **4(9)** 1–19.

Tatsumi Y, Furukawa Y and Yamashita S 1994 Thermal and geochemical evolution of the mantle wedge pin the Northeast Japan Arc. Contributions from experimental petrology; *J. Geophys. Res.* **99** 22,275–22,283.

Taylor R N, Nesbitt R W, Vidal P, Harmon R S, Auvray B and Croudace I W 1994 Mineralogy, Chemistry, and Genesis of the Boninite Series Volcanics, Chichijima, Bonin Islands, Japan; *J. Petrol.* **35** 577–617, https://doi.org/10.1093/petrology/35.3.577.

Ubide T and Kamber B S 2018 Volcanic crystals as time capsules of eruption history; *Nat. Commun.* **9** 326.

Ubide T, Cora A M, Chew D M and Kamber B S 2015 High-resolution LA-ICP-MS trace element mapping of igneous minerals: In search of magma histories; *Chem. Geol.* **409** 157–168.

Ulmer P 2001 Partial melting in the mantle wedge – the role of H_2O in the genesis of mantle-derived 'arc-related' magmas; *Phys. Earth Planet. Int.* **127(1–4)** 215–232.

Vanderhaeghe O, Ledru P, Denis T, Egal E, Cocherie A, Tegyey M and Milési J P 1998 Contrasting mechanism of crustal growth Geodynamic evolution of the Paleoproterozoic granite–greenstone belts of French Guiana; *Precamb. Res.* **92** 165–193.

Walraven F, Armstrong R A and Kruger F J 1990 A chronostratigraphic framework for the north central Kaapvaal craton, the Bushveld Complex and the Vredefort structure; *Tectonophys.* **171(1–4)** 23–48.

Winchester J G F and Floyd P A 1977 Geochemical discrimination of the magma series and their differentiation products using immobile elements; *Chem. Geol.* **20** 325–343.

Windley B F, Kusky T and Polat A 2021 Onset of plate tectonics by the Eoarchean; *Precamb. Res.* **352** 105980, ISSN 0301-9268, https://doi.org/10.1016/j.precamres.2020.105980.

Yedekar D B, Jain S C, Nair K K and Dutta K K 1990 The Central Indian collision suture; *GSI Spec. Publ.* **28** 1–43.

Corresponding editor: Somnath Dasgupta